We are IntechOpen, the world's leading publisher of Open Access books Built by scientists, for scientists

6,900
Open access books available

185,000
International authors and editors

200M
Downloads

Our authors are among the

154
Countries delivered to

TOP 1%
most cited scientists

12.2%
Contributors from top 500 universities

WEB OF SCIENCE™

Selection of our books indexed in the Book Citation Index in Web of Science™ Core Collection (BKCI)

Interested in publishing with us?
Contact book.department@intechopen.com

Numbers displayed above are based on latest data collected.
For more information visit www.intechopen.com

Chapter 8

Holographic Optical Elements to Generate Achromatic Vortices with Ultra-Short and Ultra-Intense Laser Pulses

María-Victoria Collados, Íñigo J. Sola,

Julia Marín-Sáez, Warein Holgado and Jesús Atencia

Additional information is available at the end of the chapter

http://dx.doi.org/10.5772/66314

Abstract

The requirements for the generation of optical vortices with ultra-short and ultra-intense laser pulses are considered. Several optical vortice generation procedures are analysed, specifically those based on diffractive elements, such as computer generated holograms (CGH). Optical vortices achromatization techniques are studied. Volume phase holographic (VPH) elements are considered for highly efficient, broad spectrum, high damage-threshold generation of vortices. VPH compound systems, including a compact one, for achromatic vortex generation are presented. Experimental results of vortice generation with ultra-short and ultra-intense pulses are shown.

Keywords: optical vortex, pulse shaping, volume phase holograms (VPH), aberration compensation, holographic optical elements

1. Introduction

An optical vortex is a wave that has a phase singularity, so that the intensity figure is ring-shaped, with zero intensity at the centre due to the indeterminacy of phase at that point. The phase varies helically around the singularity, from 0 to $2\pi m$, m being an integer called the *topological charge*. This kind of beams is associated with an amount of angular momentum, which makes them very attractive for certain types of applications, such as the development of optical tweezers [1]. Another application of interest is the vortex coronagraphy, which allows astronomers to create a blind spot that blocks the starlight revealing orbiting bodies such as planets or dust clouds [2], a technique that requires achromatic elements.

INTECH
open science | open minds

© 2017 The Author(s). Licensee InTech. This chapter is distributed under the terms of the Creative Commons Attribution License (http://creativecommons.org/licenses/by/3.0), which permits unrestricted use, distribution, and reproduction in any medium, provided the original work is properly cited. CC BY

In recent years interest in the generation of vortices from ultra-short and ultra-intense pulses has been increased, opening access to the experimental study of phenomenology in vortex propagation in non-linear regime [3, 4] and their possible applications, such as remote laser-induced breakdown spectroscopy (LIBS) [5], or phase control in higher order harmonics generation. The generation of high-energy vortices from ultra-intense and ultra-short laser pulses requires elements that, on the one hand, have a high damage threshold and, on the other, are able to work with a wide bandwidth.

There are several techniques for generating vortices with short laser pulses, all extrapolated from their use in continuous-wave regime, under conditions of monochromaticity and low energy. One of them is the use of modal converters, in which a vortex can be obtained from a HG_{01} mode with a combination of cylindrical lenses [6]. This technique is not feasible in the case of intense laser pulses, since it is difficult in this case to get the laser to emit in HG_{01} mode. There are modal converters based on LCD spatial light modulators, but are not applicable to high-energy lasers because of their damage threshold [7].

To date, there are two vortex generation techniques applicable to femtosecond lasers. The first is the use of spiral phase masks, manufactured either by depositing quartz onto a quartz substrate [8], by lithography in resins [9] and photoresists [10] or directly by carving on fused silica. In all cases, the mask is made with steps; the thickness increases with the azimuth angle and therefore the output phase varies helically. This type of masks has an efficiency of approximately 55% in the case of manufacturing by deposition or up to 80% in the case of photoresist, and they have a high damage threshold, allowing illumination with ultra-intense pulses obtaining high-energy vortices. A disadvantage of these phase masks is that they have some chromatic aberration when the half-width of the pulse is greater than 40 nm, which is manifested in the variation of the topological charge of the vortex with the wavelength, which limits their use to pulses higher than 30 fs [11].

Recently, Swartzlander [12] proposed a solution to try to achromatize this type of elements, by joining two different materials bonded together with a spiral phase (achieved by varying thickness) between them. With this method, achromatization is achieved for two wavelengths. In any case, the manufacturing process is expensive and requires photolithography facilities, vapour deposition or spin coating, the achromatization that can be achieved depends on the materials used and not total achromatization for the entire bandwidth is achieved.

The second technique uses computer generated holograms (CGH). In this case, the transmission gratings have a dislocation that generates the vortex and are usually printed on transparency or recorded in photographic film [13].

The efficiency of such amplitude masks is low, 6%, but may be increased by applying them a bleaching process [14] or generating patterns directly on LCD [15]. The main disadvantage of this type of dislocation gratings is the low damage threshold, which does not allow its use with high intensities. An interesting solution is the one proposed by Sacks et al. [16], which, using the vortex generated with an amplitude mask, records a volume and phase hologram with a reference plane wave, obtaining high efficiency elements.

To prevent the angular chromatic dispersion inherent to diffractive elements, a combination of two gratings with two lenses may be disposed, so that the chromatic dispersion introduced by

http://dx.doi.org/10.5772/66314

the grating with dislocation is compensated and the vortex generated is achromatic [17, 18]. Sola et al. [19] performed an assembly similar to that of Mariyenko et al. [17], replacing printed or photographed gratings with volume holographic gratings. A holographic dislocation grating was achieved by the interference of a plane wave with a vortex generated by an amplitude grating, by a procedure similar to that described by Sacks et al. [16]. The material used was dichromated gelatin (Slavich PFG04), with which highly efficient gratings were achieved and with a high damage threshold [20]. In this work, high-energy vortices were generated with a femtosecond laser, so that non-linear vortex propagation effects in air could be observed. The fundamental problem is the complexity of the assembly, which should include a vacuum chamber between the two lenses to avoid non-linear effects in the beam concentration.

There are other solutions, such as those proposed by Martínez-Matos et al. [21], in which the generation of femtosecond paraxial beams with a combination of only two volume gratings separated by some distance is proposed. The disadvantage of this solution is that the separation of gratings introduces a temporal and a spatial chirp at the ends of the Gaussian intensity profile. Atencia et al. [22] have recently developed a compact achromatic holographic vortex generator design based on attached gratings, built from a CGH. The holographic element obtained completely avoids the presence of spatial chirp across the beam intensity profile.

In this chapter the recording of volume holographic elements for the generation of vortices and two achromatization techniques with different features will be explained. In all cases the achromatism condition for a continuous bandwidth is met.

2. Basics on volume holography

2.1. Holographic recording and reconstruction

Holography is a method for recording the amplitude and phase of a wave $U_o(x,y)$ (named *object wave*) along with a reference coherent wave $U_r(x,y)$ on an intensity sensitive medium. The recording of the interference of both waves is called a hologram and the object wave can be recovered from it. The method consists of two stages: recording and reconstruction.

The complex amplitude at each point of the hologram is the sum of the amplitude of the two waves,

$$U(x,y) = U_o(x,y) + U_r(x,y) = A_o e^{-i\phi(x,y)} + A_r e^{-i\varphi(x,y)} \tag{1}$$

so intensity will be given by

$$\begin{aligned} I(x,y) &= U(x,y)\cdot U^*(x,y) = U_o U_o^* + U_r U_r^* + U_o U_r^* + U_r U_o^* \\ &= A_o^2 + A_r^2 + A_o A_r e^{-i\phi} e^{i\varphi} + A_o A_r e^{i\phi} e^{-i\varphi} \\ &= A_o^2 + A_r^2 + 2A_o A_r \cos\left[\phi(x,y) - \varphi(x,y)\right] \end{aligned} \tag{2}$$

It can be seen that the intensity varies harmonically with the phase difference. This intensity pattern is recorded in a photosensitive medium, so its transmittance changes. Assuming the

amplitude transmittance is linear with exposure of the recording material and that the intensity of the reference wave is uniform over the holographic plate, the transmittance of an amplitude hologram is given by

$$\tau(x,y) = \tau_0 + \gamma\{A_o^2 + 2A_oA_r\cos[\phi(x,y) - \varphi(x,y)]\} \tag{3}$$

where τ_0 is the uniform transmittance due to constant exposure of the reference wave and γ is the slope of the curve of transmittance versus exposure in the linear region. If the recorded hologram is illuminated with a wave with wavelength equal to the one of the recorded reference wave, the amplitude of the transmitted wave will be

$$\begin{aligned} U_i(x,y) &= U_r \cdot \tau(x,y) \\ &= (\tau_0 + \gamma A_o^2)A_r e^{i\varphi(x,y)} + \gamma A_o A_r^2 e^{-i\phi(x,y)} + \gamma A_o A_r^2 e^{i\phi(x,y)} e^{-i2\varphi(x,y)} \\ &= U_1(x,y) + U_2(x,y) + U_3(x,y) \end{aligned} \tag{4}$$

Due to the linearity of Maxwell's equations each of the addends can be interpreted as an independent wave. $U_1(x,y)$ is the beam transmitted by the hologram; it is a replica of the reference wave and corresponds to the 0 diffracted order. $U_2(x,y)$ is a replica of the object wave and corresponds to the +1 diffraction order. $U_3(x,y)$ is similar to the object wave conjugate and corresponds to the −1 diffraction order.

2.2. Volume phase holograms (VPH)

If a suitable material is used in the recording of the hologram, the intensity variations can be translated into variations of the refractive index, so that a phase hologram is recorded. In phase gratings, modulation of the refractive index is given by

$$n(x,y) = n_0 + n_1 \sin(\vec{K} \cdot \vec{r}) \tag{5}$$

where n_0 is the average index, n_1 is the amplitude modulation of the refractive index and $\vec{K}$ is the grating vector.

Consider a hologram region as shown in **Figure 1**. The holographic grating at this zone is recorded with an object wave with wave vector $\vec{k}_o$ and a reference wave with $\vec{k}_r$. The grating vector is determined with $\vec{K} = \vec{k}_o - \vec{k}_r$, and the distance between planes of constant index is $\Lambda = 2\pi/K$.

According to the relationship between the thickness d of the emulsion and the spatial period Λ of the grating thin holograms ($d \leq \Lambda$) and volume ones ($d \gg \Lambda$) can be distinguished. While in a thin hologram the three diffracted orders of Eq. (4) appear, in a volume hologram only diffracted orders 0 and +1 (U_1 and U_2 terms of Eq. (4)) are obtained.

The criterion to determine whether a hologram is volume type is given by the Q parameter,

$$Q = \frac{2\pi\lambda d}{n_0\Lambda^2} \tag{6}$$

where λ is the wavelength of the reconstruction beam. A volume hologram is considered when $Q \geq 10$.

http://dx.doi.org/10.5772/66314

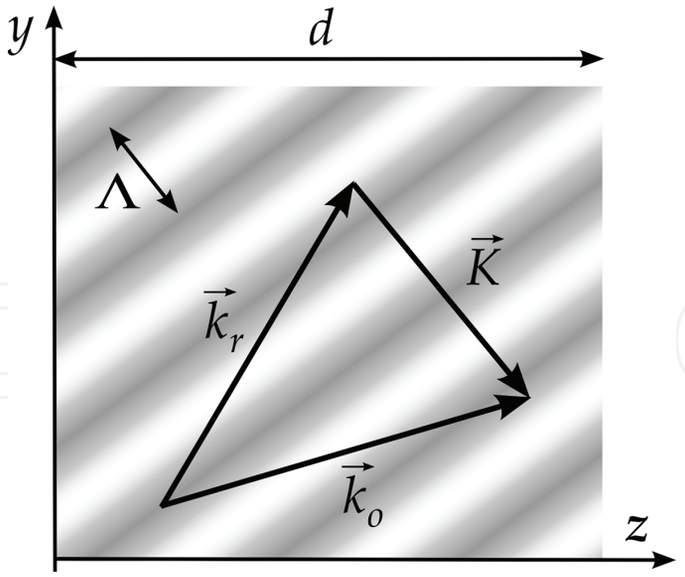

Figure 1. Volume transmission grating with object and reference wavevectors $\vec{k}_o$ and $\vec{k}_r$ and grating vector $\vec{K}$. The planes with constant refractive index, perpendicular to the grating vector, are marked with equal grey levels.

The main advantage of volume phase holograms (VPH) is that, for a given wavelength, it is possible to get 100% of the incident light diffracted to +1 order. For this to happen the so-called *Bragg condition* given by

$$2n_0\Lambda \sin\theta_0 = \lambda \tag{7}$$

must meet, where θ_0 is the half angle between the wave vectors of the incident wave $\vec{\rho}$ and the diffracted wave $\vec{\sigma}$, as shown in **Figure 2(a)**.

While the volume grating determines the energy performance, the surface grating determines the geometric behaviour. So, if in the reconstruction step a wave whose propagation vector is $\vec{\rho}$ reaches the hologram, the propagation vector $\vec{\sigma}$ of the diffracted wave must meet the following relationship:

$$\sigma_y = \rho_y \pm K_y \tag{8}$$

The distribution of energy between $\vec{\sigma}$ and $\vec{\rho}$ waves at the exit of the medium depends on the characteristics of the hologram itself and the conditions of reconstruction. The diffraction efficiency η is defined as the fraction of energy of the incident wave that is diffracted by the holographic grating.

If light hits the surface of the hologram at an angle other than θ_0, or at θ_0 but with a different wavelength, the Bragg condition is not fulfilled. Diffracted wave $\vec{\sigma}$ satisfies the geometric condition (Eq. (8)), as seen in **Figure 2(b)**. According to Kogelnik's Coupled Wave Theory [23], the efficiency when reconstructing transmission VPH near Bragg condition, is given by

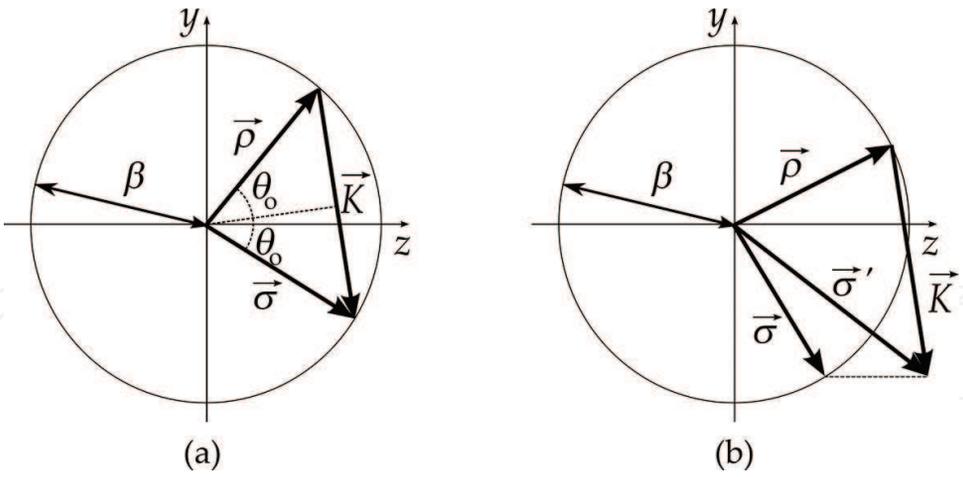

Figure 2. Wave vectors of the incident and diffracted waves and grating vector when the Bragg condition (a) is fulfilled and when (b) it is not fulfilled.

$$\eta = \frac{\sin^2(\sqrt{\nu^2 + \xi^2})}{1 + \xi^2/\nu^2} \tag{9}$$

where ξ, ν are dimensionless parameters defined as

$$\nu = \frac{\pi n_1 d}{\lambda \sqrt{c_r c_s}} \tag{10}$$

$$\xi = \frac{\vartheta d}{2c_s} \tag{11}$$

c_r and c_s are the so called *obliquity coefficients*; they are the z-component of the unit vectors in the direction of $\vec{\rho}$ and $\vec{\sigma}$, respectively. For transmission holograms, $c_s > 0$. The parameter ϑ is called *phase shift* and measures the deviation from the Bragg condition (**Figure 2(b)**). It is defined as

$$\vartheta = \frac{|\vec{\rho}|^2 - |\vec{\sigma}'|^2}{2|\vec{\rho}|} = \frac{\beta^2 - \sigma'^2}{2\beta} \tag{12}$$

with $\vec{\sigma}' = \vec{\rho} + \vec{K}$ and $\beta = 2\pi n_0/\lambda$. If the Bragg condition is strictly fulfilled (monochromatic light of wavelength λ reaches the hologram at an angle θ_0), then $\vartheta = 0$ and $\xi = 0$ and the efficiency is

$$\eta(\vartheta = 0) = \sin^2 \nu \tag{13}$$

A 100% efficiency can be achieved if the value of ν for the reconstruction wavelength λ is forced to be $\pi/2$.

When the reconstruction conditions move away from the Bragg condition the ξ parameter increases and the efficiency decreases. For polychromatic illumination (ultra-short pulses, for example), Bragg condition can be fulfilled only for a certain wavelength. To analyse the effect

http://dx.doi.org/10.5772/66314

of this in the performance of the holographic element, a polychromatic reconstruction wave of wavelength $\lambda = \lambda_0 + \Delta\lambda$ with an incident direction that meets the Bragg condition for λ_0 is considered. Usually it is assumed that $\Delta\lambda \ll \lambda_0$ [24] but for pulsed waves it is necessary to consider a broad spectrum, so $\Delta\lambda \approx \lambda_0$. Taking into account this fact, a relation between the diffraction efficiency (Eq. (9)) and the reconstruction wavelength λ can be obtained.

In ν parameter expression (Eq. (10)) only the wavelength changes, d does not vary and n_1 can be chosen to have 100% efficiency for λ_0. The obliquity factors c_r and c_s depend on the direction of illumination, determined with the Bragg condition for λ_0, so both remain constant. From these conditions,

$$\frac{\pi}{2}\lambda_0 = \frac{\pi n_1 d}{\sqrt{c_r c_s}} = cte. \tag{14}$$

So, for a wavelength λ,

$$\nu = \frac{\pi}{2}\frac{\lambda_0}{\lambda} \tag{15}$$

For ξ parameter (Eq. (9)) it is necessary to expand ϑ from Eq. (12). Taking into account **Figure 2** for an incident wave with angle θ_0 that fulfils Bragg condition for λ_0,

$$\begin{aligned} \beta^2 - \sigma'^2 &= \beta^2 - (\vec{\rho} - \vec{K})^2 = 2\vec{\rho}\vec{K} - K^2 = \\ &= 2\beta K \cos\left(\frac{\pi}{2} - \theta_0\right) - K^2 = 2\beta K \sin\theta_0 - K^2 \end{aligned} \tag{16}$$

So the phase shift ϑ is

$$\vartheta = \frac{2\beta K \sin\theta_0 - K^2}{2\beta} \tag{17}$$

From the Bragg condition for λ_0 the following relationship is obtained,

$$2n_0\Lambda \sin\theta_0 = \lambda_0 \tag{18}$$

Replacing Eq. (18) in Eq. (17) and substituting the expression of β,

$$\vartheta = \frac{K^2(\lambda_0 - \lambda)}{4\pi n_0} \tag{19}$$

To have the widest possible diffracted spectrum a small angle between beams is used, and wave vectors near the normal direction are chosen, so $c_s \approx 1$, and ξ parameter (Eq. (11)) is

$$\xi = \frac{K^2 d(\lambda_0 - \lambda)}{8\pi n_0} \tag{20}$$

Substituting the obtained values of ξ and ν in Eq. (9) the efficiency as a function of the reconstruction wavelength for a broad spectrum ($\Delta\lambda \approx \lambda_0$) is obtained.

A numerical simulation of the spectrum diffracted by a holographic grating has been carried out with typical values for ultra-short pulses (λ_0 = 800 nm) and for dichromated gelatin Slavich PFG04 commercial plates [20] (d = 30 μm and $n_0 = 1.52$). In the volume hologram limit, for Q = 10, a grating period of $\Lambda = 3.15\ \mu$m is obtained. The graph of efficiency vs. reconstruction wavelength is shown in **Figure 3**. It can be seen that the efficiency is higher than 90% for a band with $\Delta\lambda = \pm 100$ nm, so this type of VPH could be adequate for its use with ultra-short pulses.

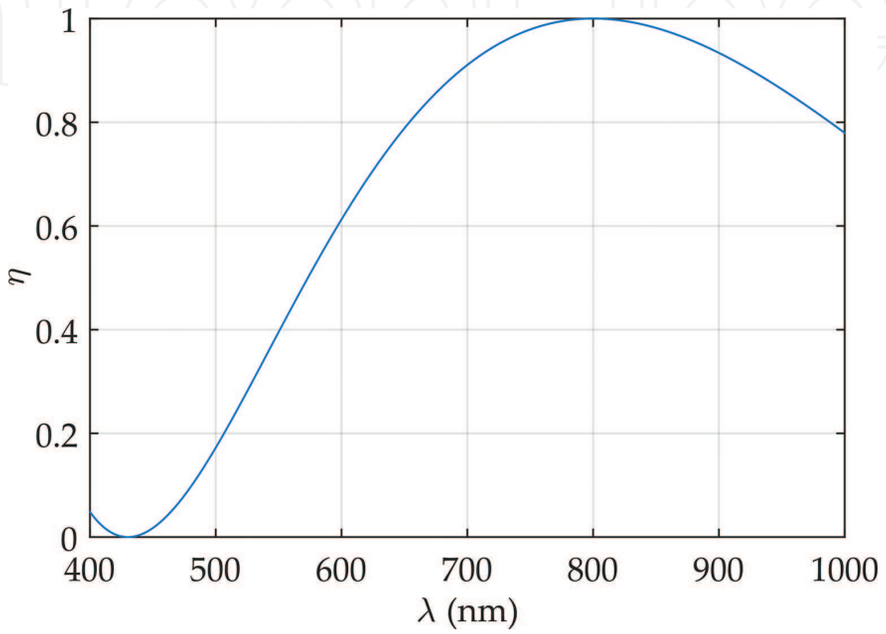

Figure 3. Theoretical efficiency of a transmission VPH as a function of the reconstruction wavelength for $\lambda_0 = 800$ nm, $d = 30\ \mu$m, $n_0 = 1.52$, $Q = 10$.

3. Vortex generation with holographic optical elements

A holographic vortex generation element is recorded by the interference of a plane (or spherical) wave and a vortex beam. Since the recording is with monochromatic light, any of the methods described in Section 1 can be used to generate this vortex object wave. For this work a computer generated hologram (CGH) was chosen.

In order to generate the CGH, the interference between a plane wave (reference wave), with its wave vector forming an angle α_1 with the z-axis, and a vortex-carrying plane wave (object wave), which propagates in the z-axis, is calculated. The reference plane wave at the hologram plane can be expressed as

$$U_r(x,y) = \mathrm{e}^{-i\frac{2\pi}{\lambda}x\sin\alpha_1} \tag{21}$$

and the object vortex wave as

$$U_o(x,y) = \mathrm{e}^{-im\theta} \tag{22}$$

http://dx.doi.org/10.5772/66314

where $\theta = \tan^{-1}(y/x)$ is the angular coordinate at the hologram plane. The intensity distribution on the CGH is given by

$$I = |U_r + U_o|^2 = 2\left[1 + \cos\left(\frac{2\pi}{\lambda} x \sin\alpha_1 + m\theta\right)\right] \tag{23}$$

λ and α_1 are chosen to obtain the desired spatial period $\Lambda = \lambda/\sin\alpha_1$. The intensity distribution is calculated with MatLab, binarized, and printed on paper with a laser printer to obtain a grating with dislocation. **Figure 4** shows a CGH calculated for $m = 1$.

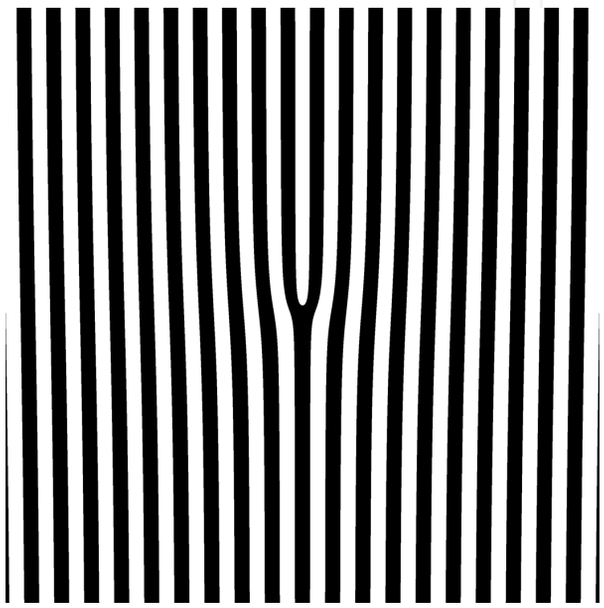

Figure 4. Dislocated grating obtained with the interference of a plane wave and a vortex wave with topological charge $m = 1$.

The printed pattern is photographically reduced using a reflex camera with Kodak TMax100 film, obtaining an amplitude thin grating of 14.7 lines/mm with a dislocation at the centre. This CGH has high absorption, so it cannot be illuminated with a high-intensity laser, because it could be damaged. Therefore the resulting film is contact-copied onto a commercial Slavich PFG04 dichromated gelatin plate using incoherent light. After this complex procedure a thin phase CGH is obtained. It can be illuminated with an intense laser, although multiple diffracted orders are obtained and their efficiency is low (25%).

The CGH is used to generate the object wave for the recording of a VPH. The recording scheme is shown in **Figure 5**. The beam of a Coherent Verdi 6 W CW laser emitting at 532 nm is divided in two by means of a beam splitter BS. One of the beams is filtered and expanded with a spatial filter and collimated with a lens L_1, and acts as a plane reference beam. The other beam is first filtered and expanded and then collimated with a lens L_2, and illuminates the thin phase CGH. The effects of bitmap resolution in the previous laser-printed CGH require to use spatial filtering techniques to select the desired diffraction order and to avoid bitmap artefacts [16]. The +1 diffracted order, containing the vortex, is selected, filtered and imaged with magnification

$-f_4/f_3$ onto the recording plate to cancel phase propagation terms by means of the 4-*f* processor formed with lenses L_3 and L_4. Slavich PFG04 dichromated gelatin plates are used, following the process described in [20] to obtain maximum efficiency at 800 nm. The two recording beams form an angle of 10°, the minimum angle required to obtain a volume hologram ($Q = 10$) with the 30 μm-thick PFG04 emulsion.

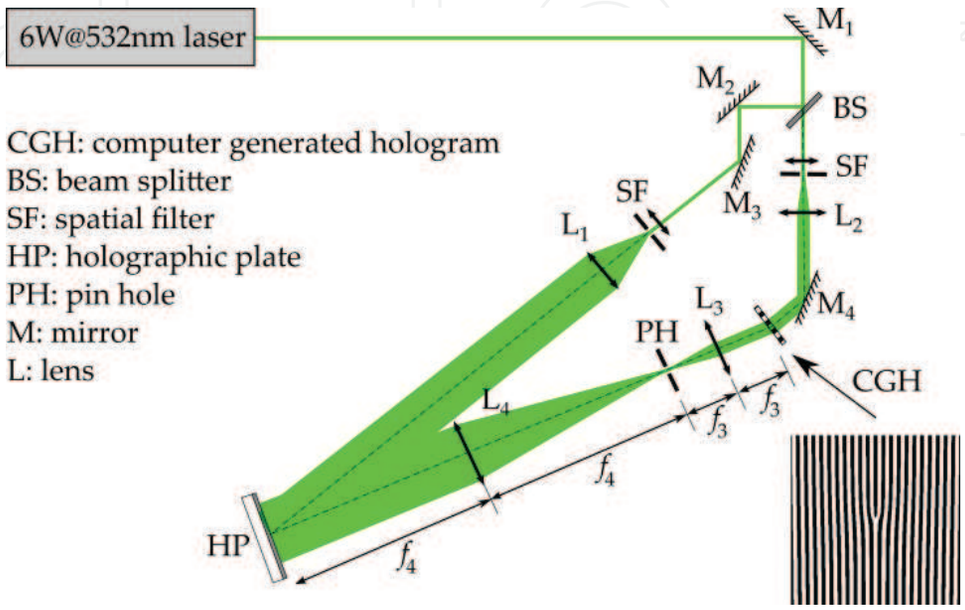

Figure 5. Scheme of the recording setup of a volume holographic optical element with a vortex-carrying plane wave as object wave.

The recorded VPH presents an efficiency of 95% at 800 nm. The spatial period is $\Lambda = 2.93$ μm that corresponds to 340 lines/mm spatial frequency. The diffracted spectrum is shown in **Figure 6**. It can be seen that the maximum efficiency appears for 800 nm, and the wavelength

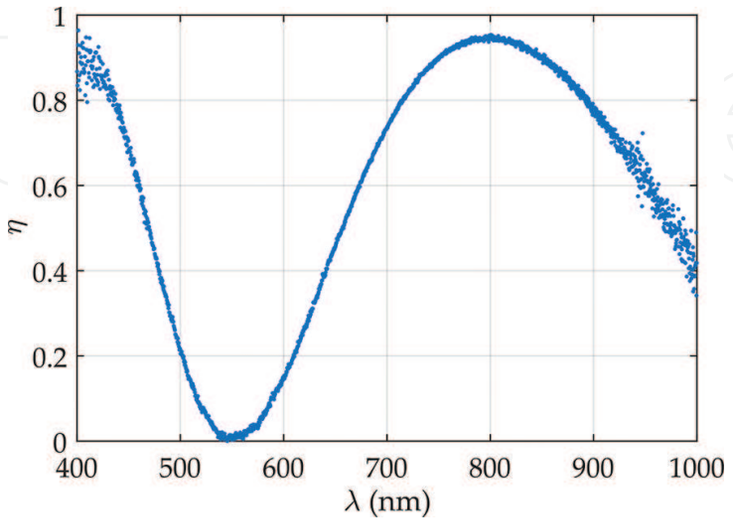

Figure 6. Efficiency of the +1 diffraction order of the recorded VPH as a function of the reconstruction wavelength.

http://dx.doi.org/10.5772/66314

range in which the diffractive efficiency is above 80%, is almost 200 nm. The holographic material Slavich PFG04 has high damage threshold [25], so the recorded VPH can be used with ultra-short and ultra-intense laser pulses.

In **Figure 7**, the Fourier transform of the vortex generated by the VPH when illuminated with a CW laser beam of 800 nm is shown.

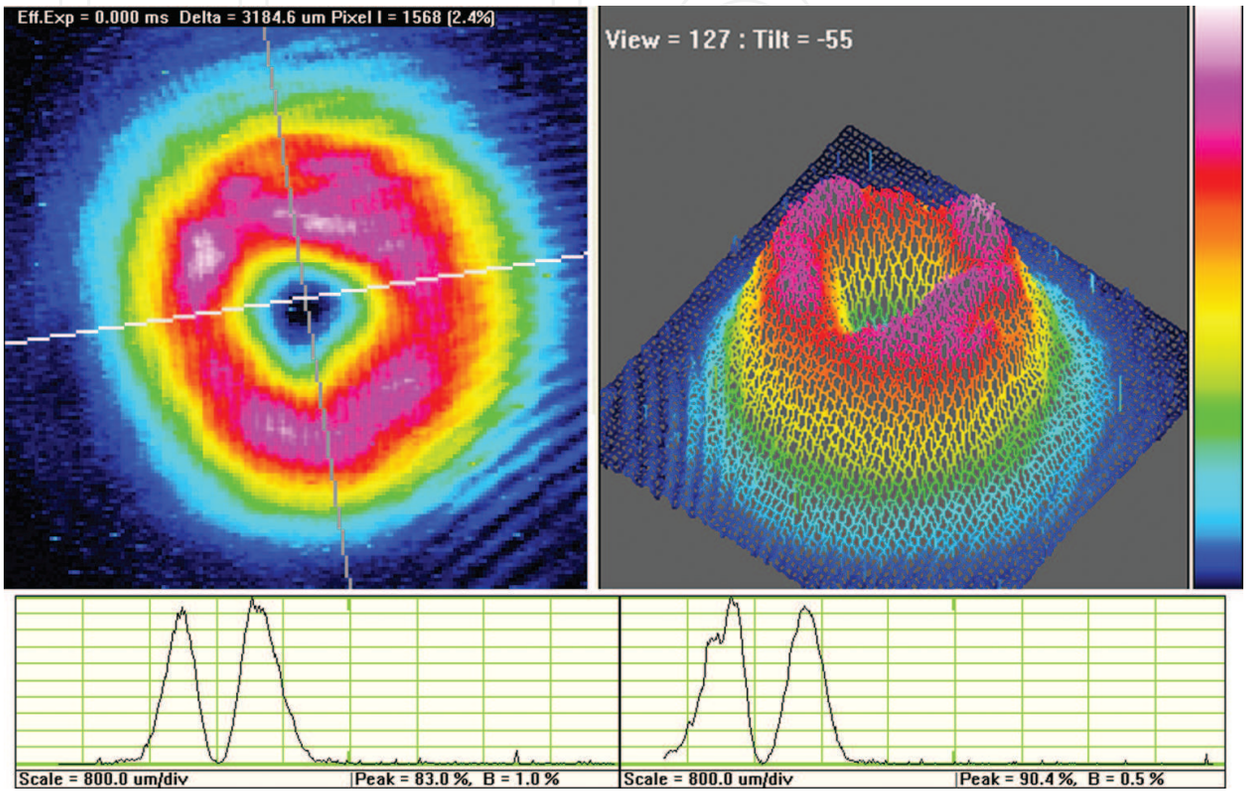

Figure 7. Fourier transform of the vortex generated by the VPH when illuminated with a CW laser beam of 800 nm.

4. Holographic generation of achromatic vortex beams

A disadvantage of using the previous holographic optical element to generate vortex beams with ultra-short pulses is the chromatic dispersion. As we have seen, the VPH can work properly in a spectral range of around 200 nm, but the direction of the diffracted vortex beam depends on the wavelength, so the vortex beam presents an important spatial chirp, as it is shown in **Figure 8**.

This problem can be overcome by designing an achromatic set-up in which the chromatic dispersion of the vortex beam is compensated by using a volume holographic plane grating (H_I) with the same spatial frequency as the vortex generator VPH (H_{II}).

H_I is recorded with two plane waves of wavelength λ' that propagate forming an angle α_o and α_r with z-axis, so the complex transmittance of the grating (Eq. (3)), considering a phase hologram, is proportional to

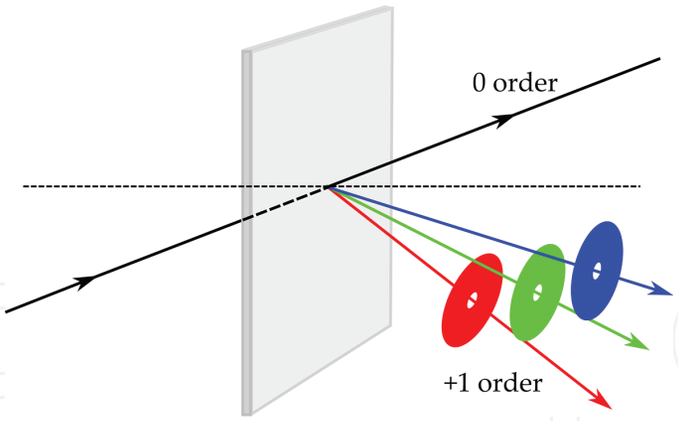

Figure 8. Chromatic dispersion of the vortex generator VPH described in Section 3.

$$\tau_I(x,y) = 1 + \frac{1}{2}e^{i\frac{2\pi}{\lambda'}x\ (\sin\alpha_r - \sin\alpha_o)} + \frac{1}{2}e^{-i\frac{2\pi}{\lambda'}x\ (\sin\alpha_r - \sin\alpha_o)} \tag{24}$$

H_{II} is recorded with the interference of a plane wave, forming an angle α_r with z-axis, and a vortex beam forming an angle α_o with z-axis, so the complex transmittance of H_{II} is given by

$$\tau_{II}(x,y) = 1 + \frac{1}{2}e^{i\left(\frac{2\pi}{\lambda'}x\ (\sin\alpha_r - \sin\alpha_o) + m\theta\right)} + \frac{1}{2}e^{-i\left(\frac{2\pi}{\lambda'}x\ (\sin\alpha_r - \sin\alpha_o) + m\theta\right)} \tag{25}$$

4.1. Achromatization with separated elements

The first approach to combine these two VPH is proposed by Sola et al. [19] based on a solution with printed gratings suggested by Mariyenko et al. [17]. H_{II} is located at the plane where a positive lens (L_1) forms the image of the grating H_I in a 2*f*-2*f* configuration, as shown in **Figure 9**.

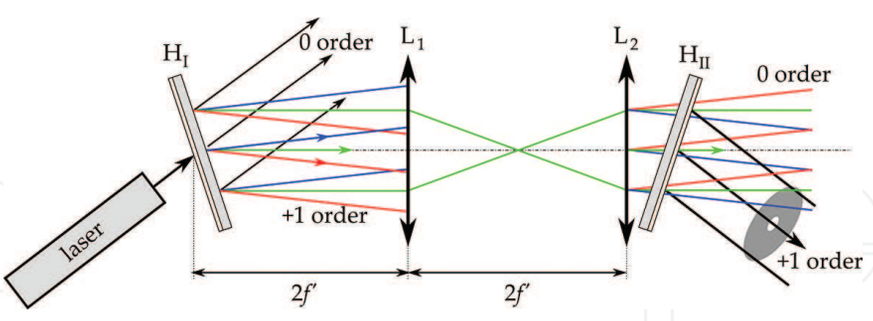

Figure 9. Scheme of the experimental set-up for generating vortices with separated holographic elements.

If we consider that H_I is illuminated with a polychromatic plane wave with a Gaussian spatial profile, $U_c(x,y)$,

$$U_c(x,y) = \int_{-\infty}^{\infty} u(\lambda) e^{-\frac{(x^2+y^2)}{w^2}} e^{-i\frac{2\pi}{\lambda}x\ \sin\alpha_c} d\lambda \tag{26}$$

where $u(\lambda)$ is the wave spectrum and w is the half wide of the Gaussian beam, then the wave emerging from H_I, $U_{i,I}(x,y)$, can be expressed as

http://dx.doi.org/10.5772/66314

$$
\begin{aligned}
U_{i,I}(x,y) &= U_C(x,y)\cdot\tau_I(x,y) = \\
&= \int_{-\infty}^{\infty} u(\lambda)\mathrm{e}^{-\frac{(x^2+y^2)}{w^2}}\mathrm{e}^{-i\frac{2\pi}{\lambda}x\ \sin\alpha_c}\mathrm{d}\lambda + \\
&+\frac{1}{2}\int_{-\infty}^{\infty} u(\lambda)\mathrm{e}^{-\frac{(x^2+y^2)}{w^2}}\mathrm{e}^{-i\left\{\frac{2\pi}{\lambda}x\left[\ \sin\alpha_c-\frac{\lambda}{\lambda'}(\sin\alpha_r-\sin\alpha_o)\right]\right\}}\mathrm{d}\lambda + \\
&+\frac{1}{2}\int_{-\infty}^{\infty} u(\lambda)\mathrm{e}^{-\frac{(x^2+y^2)}{w^2}}\mathrm{e}^{-i\left\{\frac{2\pi}{\lambda}x\left[\ \sin\alpha_c+\frac{\lambda}{\lambda'}(\sin\alpha_r-\sin\alpha_o)\right]\right\}}\mathrm{d}\lambda = \\
&= U_{1,I}(x,y)+U_{2,I}(x,y)+U_{3,I}(x,y)
\end{aligned}
\tag{27}
$$

$U_{1,I}$ is the transmitted order; $U_{2,I}$ and $U_{3,I}$ are the +1 and -1 diffracted orders, respectively. In the case of volume holograms, only one of these orders is diffracted, depending on the α_C value. In this case, the order efficiently diffracted by the VPH is $U_{2,I}$, which is a set of polychromatic plane waves with a Gaussian spatial profile. The direction of propagation of each wavelength, α_i, is a function of λ,

$$
\sin\alpha_i = \sin\alpha_c-\frac{\lambda}{\lambda'}(\sin\alpha_r-\sin\alpha_o) \tag{28}
$$

Considering L_1 as an ideal lens, the complex amplitude at the image plane $U'_{2,I}(x,y)$ is given by [26]

$$
U'_{2,I}(x,y) = \frac{1}{|M|}U_{2,I}\left(\frac{x}{M},\frac{y}{M}\right) \tag{29}
$$

where M is the magnification. In this case, as the lens L_1 works in a 2*f*-2*f* configuration, $M=-1$, so

$$
U'_{2,I}(x,y) = \frac{1}{2}\int_{-\infty}^{+\infty} u(\lambda)e^{\frac{-(x^2+y^2)}{w^2}}e^{i\left\{\frac{2\pi}{\lambda}x\left[\sin\alpha_c-\frac{\lambda}{\lambda'}(\sin\alpha_r-\sin\alpha_o)\right]\right\}}d\lambda \tag{30}
$$

$U'_{2,I}$ illuminates the second hologram H_{II}, so the amplitude distribution that leaves H_{II} is

$$
U_{i,II} = \tau_{II}U'_{2,I} = U_{1,II}+U_{2,II}+U_{3,II} \tag{31}
$$

The term $U_{2,II}$ is the efficiently diffracted order, and is given by

$$
U_{2,II} = \frac{1}{2}\int_{-\infty}^{+\infty} u(\lambda)e^{\frac{-(x^2+y^2)}{w^2}}e^{i\left\{\frac{2\pi}{\lambda}x\sin\alpha_c+m\theta\right\}}d\lambda \tag{32}
$$

$U_{3,II}$ is an achromatic vortex without chromatic dispersion, as the direction of the propagation does not depend on the wavelength.

A second lens L_2, with the same focal length as L_1, is placed just in front of or behind H_{II}, restoring the phase of the propagating beam into a plane wavefront. The VPH to generate

the vortex beam has been recorded with a plane wave as a reference wave, so placing the lens L_2 in front of H_{II} (as it is shown in **Figure 9**) provides a reconstruction plane wave, which assures the reconstruction of the vortex beam with no geometrical aberrations.

Depending on the intensity of the pulses, the use of a vacuum chamber between the two lenses could be necessary to avoid non-linear effects in the focalization produced by the lens L_1.

4.2. Achromatization with a compact element

The second approach was proposed by Atencia et al. [22]. In this case both holographic elements H_I and H_{II} are placed parallel to each other, as it can be seen in **Figure 10**.

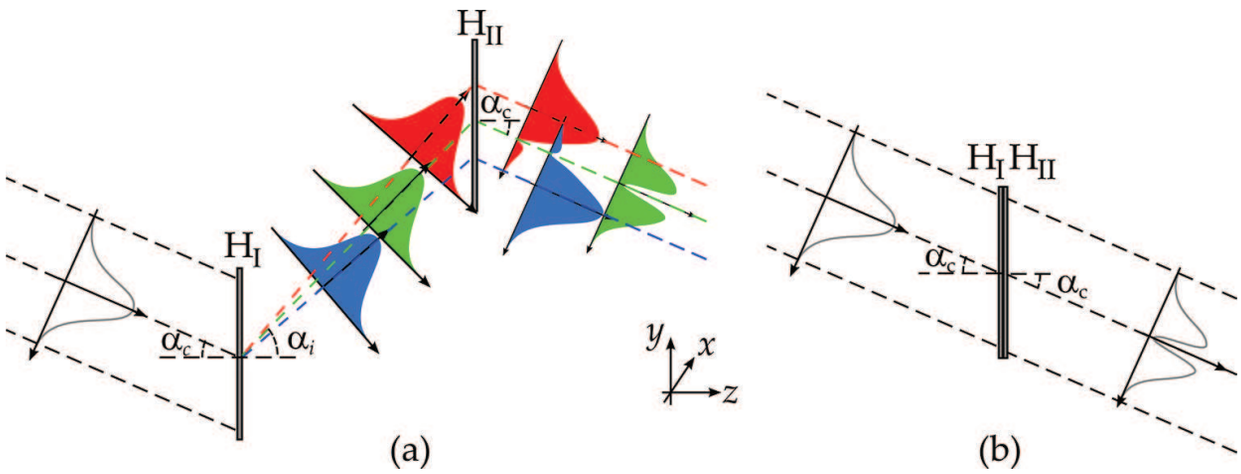

Figure 10. Double-grating vortex generator. (a) Separated VPH, (b) compact VPH.

If H_I and H_{II} are separated (**Figure 10(a)**), the Gaussian profile of the incident beam is kept in the propagation between H_I and H_{II}, but the different wavelengths are spatially separated and de-phased when they reach H_{II}. A set of vortices emerges from H_{II}, all with the same topological charge m forming the same angle with the z-axis. The position of the vortex is the same for all wavelengths, but the Gaussian distribution is spatially shifted for each wavelength.

If the two VPH are placed together, as in **Figure 10(b)**, the amplitude distribution that reaches H_{II} is $U_{2,I}$, so the distribution that leaves H_{II} is

$$U_{i,II} = \tau_{II} U_{2,I} = U_{1,II} + U_{2,II} + U_{3,II} \tag{33}$$

where, in this case, $U_{3,II}$ is the order that is diffracted efficiently and is given by

$$U_{3,II} = \frac{1}{2}\int_{-\infty}^{+\infty} u(\lambda) e^{\frac{-(x^2+y^2)}{w^2}} e^{-i\left\{\frac{2\pi}{\lambda} y \sin\alpha_c + m\theta\right\}} d\lambda \tag{34}$$

http://dx.doi.org/10.5772/66314

$U_{3,II}$ is a set of vortices emerging from H_{II}, all with the same topological charge m and forming an angle of α_c with the z-axis.

In the construction of this compact VPH, the recording scheme for H_I is similar to that shown in **Figure 5** by replacing the vortex wave with a collimated wave. The angle between beams has to be the same for H_I and H_{II} to guarantee the chromatic compensation. For a simpler alignment procedure, the recording geometry for H_I and H_{II} is chosen to give Bragg condition at 800 nm for an angle $\alpha_c = 0$.

After processing, H_I and H_{II} are cemented to each other, using Norland NOA61 optical adhesive between the two emulsions. This ensures that no change in the refraction index between the holograms occurs and preserves the emulsion from degradation effects of the environment.

When illuminating each VPH at Bragg angle for 800 nm, the maximum efficiency obtained is approximately 95%, so the sandwich has a total maximum efficiency of 90%. Reflection on glass surfaces and glass absorption causes losses of about 15%, so the compound holographic element reaches an absolute efficiency of 77%. When λ moves away from 800 nm, this efficiency decreases. For the compound element, **Figure 11** shows the wavelength dependence of the diffractive efficiency. It can be observed that the full width at half maximum (FWHM) covers 250 nm, and the diffracted efficiency is above 80% for a wavelength range of 100 nm.

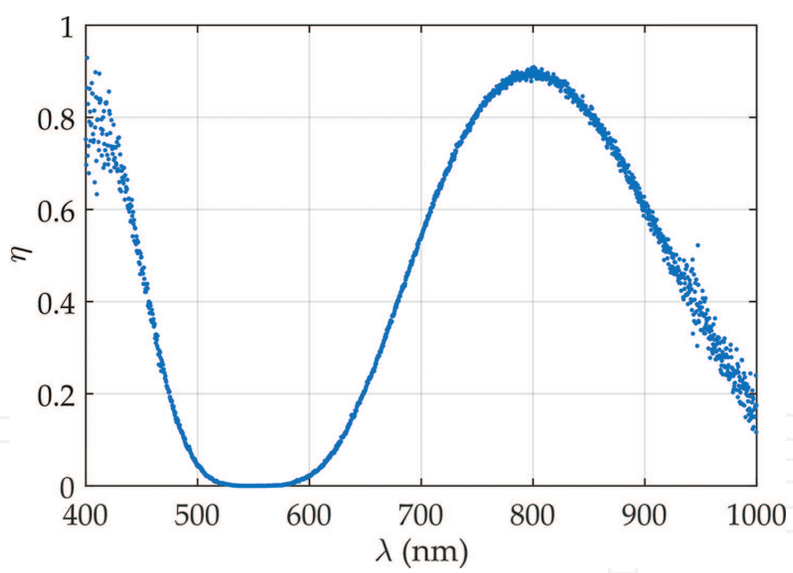

Figure 11. Dependence of the diffractive efficiency of the compact VPH with the wavelength.

For wavelengths different from 800 nm the diffractive efficiency drops and the transmitted light increases, so the transmitted and diffracted light can spatially overlap for some wavelengths. To prevent this, H_I is slightly rotated around the z-axis before joining the two holograms. So, the transmitted and diffracted beams emerge from H_{II} with different directions, but the efficiency is not affected.

Figure 12(a) and **(b)** demonstrate that the compound element generates a broadband achromatic optical vortex. A 5 mm-wide white light vortex can be seen in **Figure 12(a)**, when illuminating the compact VPH with a tungsten light source (Ocean Optics LS-1) with 600 nm FWHM centred at 850 nm. The photograph was taken at 1 m propagation from the element output. **Figure 12(b)** shows the interference of transmitted and diffracted light. To obtain an appreciable intensity on the transmitted beam, the holographic element is illuminated out of Bragg condition. The dislocation of the interference pattern is clearly visible at the centre of the image.

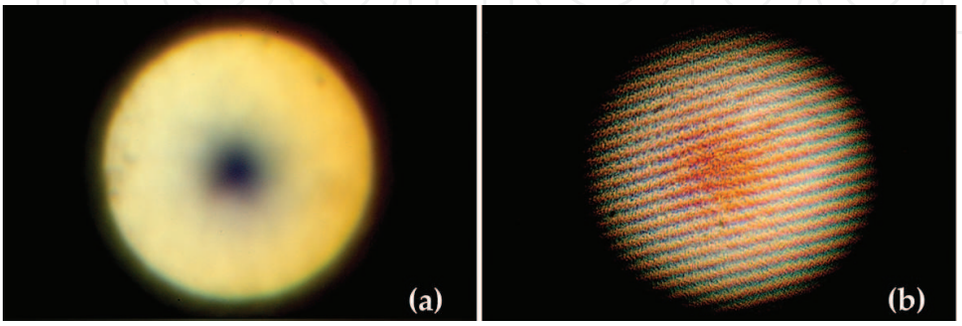

Figure 12. White light vortex. (a) Propagated at 1 m, (b) interference with a plane wave.

This compact vortex generator holographic element is very easy to align and avoids pulse concentration zones, so for ultra-intense pulses the use of a vacuum chamber is not required.

5. Applications of vortex volume phase holograms to ultra-fast optics

Once the recording process of a vortex generating VPH has been reviewed, and the two solutions for the vortex achromatization have been described, in the following section we will comment some of the characteristics of the generated vortex and some possible applications using femtosecond high power pulses. The achromatization of the VPH is very attractive from the point of view of ultra-short pulses, which present broadband spectra, allowing the generation of short vortex pulses with high peak power [19]. The main limitation to obtain shorter pulses is the spectral bandwidth of the hologram; however, the present performance allows the generation of ultra-short vortex beams (e.g., compact vortex VPH is compatible with few tenths of fs pulses).

One of the first questions arising is what the spatiotemporal structure of the vortex looks like. In the literature, fs pulse vortices generated by spiral phase masks have been characterized by using spatially resolved interferometry [27]. In the case of the compact VPH, when studying spatial pattern of interferences in a similar way, a peculiar behaviour was observed. **Figure 13** shows the interference pattern between two replicas of the laser beam (pulses of 100 fs FWHM, central wavelength at 795 nm), obtained at a Mach-Zender interferometer. One of the beams passed through a topological charge $m = 1$ compact VPH, while the other arm acted as a spatio-

http://dx.doi.org/10.5772/66314

temporal reference. As expected, fork-like interference pattern appears when both optical paths of the interferometer match, disappearing otherwise. However, a spatial evolution of the interference region is observed. Starting from a situation of unbalanced optical path length of each interferometer arms, with no visible spatial interference pattern, the time delay between the vortex pulse and the reference one is gradually reduced. When the pulse distance becomes within the coherence length, spatial interferences arise, but localized in a spatial region (**Figure 13(a)**). Reducing the arm difference increases the contrast of the interferences but it also shifts them in the diagonal direction (**Figure 13(b)–(d)**). Finally, when the optical path mismatch increases again, interferences disappear, located on the opposite region of the beam profile (**Figure 13(d)** and (**e**)). This time dependence of interference spatial regions shows that the vortex beam is generated with a pulse tilt. According to the experimental result, the tilt could be quantified around 40 fs/mm in the direction of the VPH incident beam-vortex mismatch (induced, as commented in 4.2 by the small rotation of H_I related to H_{II} in order to avoid overlapping between transmitted and diffracted beams). Similar results were obtained using pulses of 25 fs FWHM.

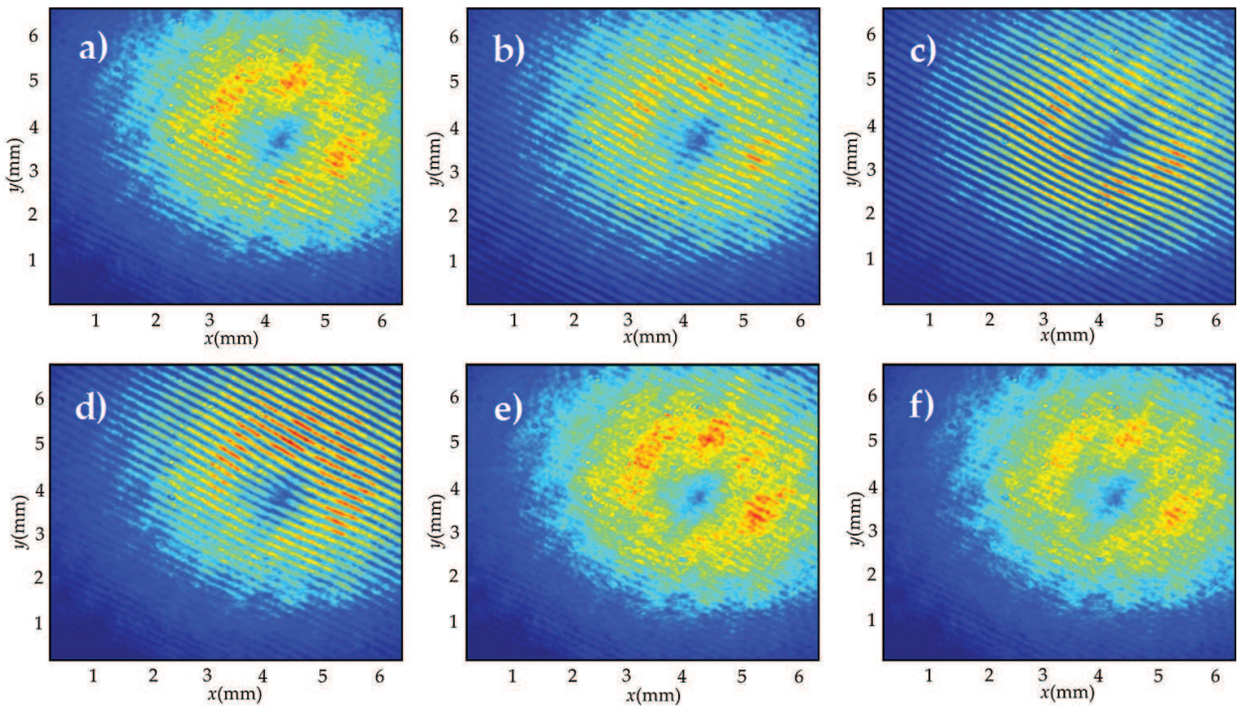

Figure 13. Interference patterns between an $m = 1$ vortex beam generated with the compact VPH described in Section 4.2 and a collimated Gaussian beam, presenting a small angle between them. The interference region varies as the relative interferometer arm delay changes (time shift between arms: 0 fs (reference) (a); 67 fs (b); 133 fs (c); 266 fs (d); 400 fs (e); 533 fs (f)).

Although this pulse tilt is small and for the most of applications it plays no relevant role (e.g., in the following non-linear interaction cases presented in this section no relevant effect has been observed), it is important to be aware of its existence. One way of reducing it would be to better match transmitted-diffracted beam directions. Nevertheless, if some of the incident beam is transmitted through the compact VPH, it may interfere with the vortex beam. On the

other hand, it has recently been shown that controlled pulse tilts can be a tool to induce interesting effects, such as the so-called attosecond lighthouses [28]. Therefore, the ability of imprinting controlled spatiotemporal alterations on the VPH may have potential applications.

One of the main advantages of using the compact VPH consists on the possibility of creating a high power vortex quite easily. The set-up for generating the high power vortices is simplified to the point of making the ultra-short pulses pass through it, while orienting the VPH in the proper angle, defined by the recording configuration. Since the element presents a high damage threshold of, at least, hundreds of GW/cm^2 [19], the incident pulse peak power can be high, allowing to generate high-power vortices because of the high efficiency of the VPH. Therefore, it makes it possible to induce non-linear effects on the vortex beams while propagating though a certain medium.

In order to explore the potential of VPH creating high intensity femtosecond vortices, different experiments have been performed. Firstly, using the achromatic set-up described in Section 4.1, the dynamics of vortices at different intensity regimes were studied [19], analysing the evolution of the spatial distribution of the light along propagation after passing through a focusing lens (f = 2.2 m). While working on low-intensity regime (linear regime), the vortex maintains its structure at focus and after it, remains stable. However, for high intensity regime the dynamics varies, as shown in **Figure 14**. The vortex structure, unaltered in the first centimetres of the focusing propagation, begins to be affected by the non-linear propagation. Just before the focus, because of the Kerr effect driven self-focusing, the vortex splits into two fragments. It is intriguing to observe how the two splinters rotate along the optical axis as the beam propagates, following a spiralling path. When the beam diverges, away from the focal region, the splinters stop from rotating. This behaviour can be explained as an effect of angular momentum conservation. Numerical calculations [19] were carried out from (2+1)-dimensional numerical simulations based on solving the non-linear Schrödinger equation including Kerr effect, as described in Ref. [29]. Agreement between theory and experiments shows the major role of the Kerr effect on the dynamics, since other possible players (as ionization) were not included on the calculations.

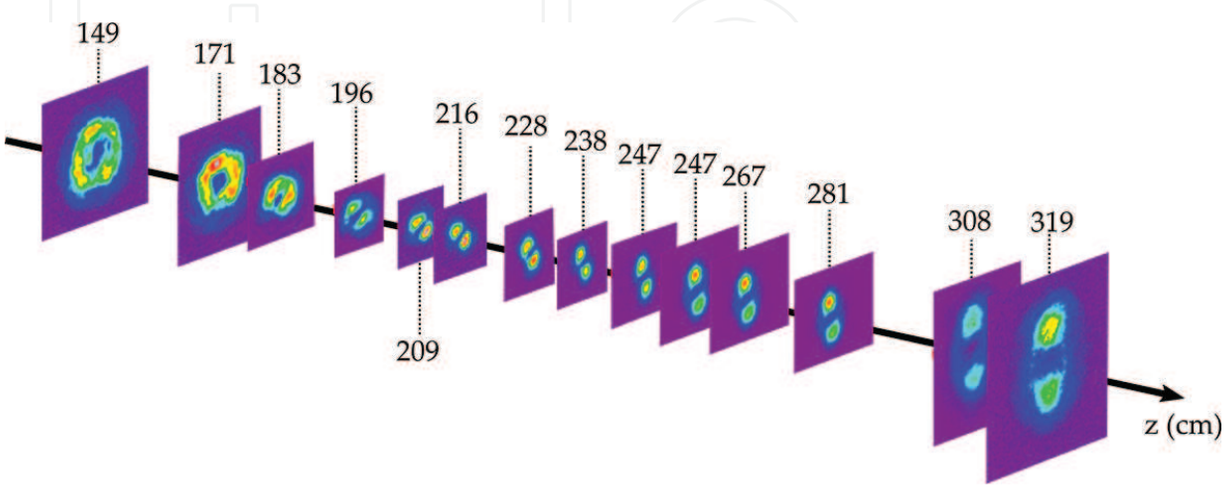

Figure 14. Spatial beam profile evolution of 14 GW vortex focused by an f = 2.2 m convergent lens.

http://dx.doi.org/10.5772/66314

An increase of beam intensity would involve utterly medium ionization. Then, light propagation may become even more complex, being the result of the interplay between effects competing for focusing or unfocusing the beam (e.g. Kerr effect will introduce focusing on the beam, while ionization makes the opposite). This may produce what is called filamentation [30], exhibiting a self-guiding of the beam because of the balance between linear regime light propagation and the different non-linear effects raised from interaction with the medium. Splitting and filamentation of the vortex fragments have been observed for high enough intensities (e.g., 14 GW vortices propagating in a tube filled with nitrogen at a pressure of 1600 mbar [19]).

In the last decades, an extremely non-linear process known as high order harmonic generation (HHG) has become a hot topic and the basis of the new discipline called *Attoscience* [31]. This process rises from the interaction of intense light and matter and enables to obtain harmonic frequencies of the driving radiation well inside the ultraviolet spectral region (known as extreme ultraviolet, or XUV) or even the soft X-ray region [32]. In the case of interaction with gases, it can be interpreted as a three-step process [33, 34], starting with matter ionization, freeing an electron (typically in tunnelling regime). In a second step, the electron is accelerated by the intense electromagnetic field of the pulse. Finally, depending on the electric-field phase, the electron may return towards the parent ion, recombining and emitting the accumulated energy (kinetic energy plus the ionization potential) as a photon. This XUV radiation inherits coherence from the generating beam, while showing a peculiar temporal emission pattern, a train of sub-femtosecond pulses. It can be eventually reduced to a single XUV burst by means of few cycle driving pulses and gating techniques [35–37]. This kind of extremely short light sources is an unprecedented tool for studying fast dynamics, as molecular or electronic [31]. Within this context, during the last years, special attention is being devoted to the HHG of pulses with orbital angular momentum (OAM), as vortices. The first experimental work showing the generation of XUV vortices from IR ones was reported on 2012 [38]. The measurements of the topological charges of the different harmonic yielded unexpectedly a constant charge $m = 1$ (coming from the same charge in the driving field), independent of the harmonic order. The authors explained this discrepancy as caused by vortex decay during the non-linear process. Later, numerical simulations [39] predicted topological charge scaling with the order of the harmonics and subsequent experiments [40] confirmed this point.

The basis of HHG and its use for the generation of XUV beams exhibiting OAM are analysed in depth in another chapter of this book [41]. Here we will focus on the use of vortex generating compact VPH in HHG experiments. In the pioneering experimental studies [38, 40], the OAM driving beam was obtained from a 30 fs pulsed beam and $m = 1$ topological charge was imprinted by means of a spatial light modulator (SLM) but using two different ways. In the case of Zürch et al. [38], the reflective SLM was used to imprint the AOM in a spiral phase mask way, introducing diphase of the wavefront phases azimuthally dependent. On the other hand, Gariepy et al. [40] used the SLM for creating a fork type diffraction pattern, i.e. presenting dislocation introducing the topological charge. In order to compensate the first order angular dispersion, a long period-grating pattern was used. This way of generating vortices allows to imprint the same topological charge to all the wavelengths, in contrast with the spiralling phase mask procedure that,

as shown in Ref. [27], produces topological charges depending on the wavelength, being even not an integer.

Therefore, the case of Gariepy et al. [40] is quite similar to the way the compact VPH generates the vortices, with a dislocated grating and a second non-dislocated grating to suppress angular dispersion. The main difference lays on the fact of using a SLM element or a holographic plate. While the former is more flexible and dynamic, the compact VPH is a more robust and cheaper element, presenting a simpler alignment.

Then, in order to explore its potential, we tested the compact VPH in a HHG experiment. The experimental set-up is shown in **Figure 15**. A 25 fs pulsed beam up to 2 mJ per pulse (1 kHz repetition rate, spectrum centred on 790 nm) is focused by means of a f = 50 cm spherical Ag mirror into an Ar gas jet on vacuum (10^{-3} mbar of residual pressure when the gas jet is operating). After light-matter interaction, radiation passes through a 4 mm long slit to a Rowland circle spectrometer (Model 248/310G, McPherson Inc.), using a 1 m radius spherical grating (133 lines/mm). A 150 nm Al filter just after the slit absorbs the fundamental radiation and lower harmonics, up to the 11th. The compact VPH was placed before the focusing element, creating the AOM beam. Because of the physical dimension of the set-up and XUV beam divergence, the size of the harmonic vortices was bigger than the slit dimensions. Therefore, several measurements were performed, shifting the height of IR beam and gas jet referred to the slit position. **Figure 16** shows the combined spectra for different divergence angle. The result shows annular distribution of the harmonics, with a minimum of intensity in the centre (divergence 0 mrad) and a ring around 3-6 mrad. Although no measurement concerning topological charge has been performed, results are compatible with the obtained at [40].

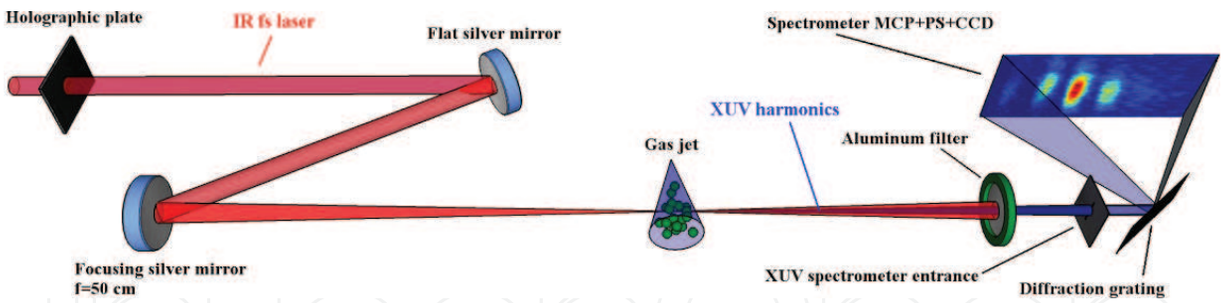

Figure 15. HHG experimental set-up for generating XUV. A 25 fs pulsed beam passes through the compact VPH (Holographic plate), creating an m = 1 vortex. The beam is focused by means of a spherical Ag mirror (f = 0.5 m) on an Ar gas jet, where HHG occurs. XUV radiation is filtered by an Al filter and spectrally analysed using a Rowland circle spectrometer (Model 248/310G, McPherson Inc.) including an spherical diffraction grating (133 lines/mm), and a detector composed by a micro-channel plate (MCP), a phosphor screen (PS) and a CCD camera.

In summary, the compact VPH [22] is a simple, cheap and robust element for generating high power AOM beams. Their achromaticity allows the generation of pulsed vortices down a few tenths of fs and their high damage threshold permits to obtain high peak powers. High power vortex generated by this way are able to interact non-linearly with material, producing effects from Kerr effect and filamentation to HHG.

http://dx.doi.org/10.5772/66314

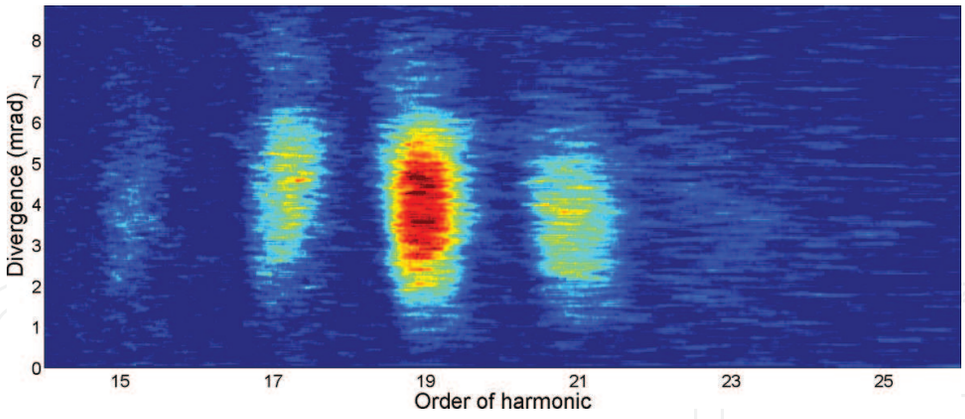

Figure 16. Spectrum of high order harmonic radiation depending on divergence, once the IR beam and lower harmonic have been filtered.

Acknowledgements

This research was supported by 'Ministerio de Economía y Competitividad' of Spain for the funding (projects FIS2013-44174-P and FIS2015-71933-REDT), Diputación General de Aragón-Fondo Social Europeo (TOL research group, T76), Junta de Castilla y León (projects SA116U13, UIC016 and SA046U16), Generalitat de Catalunya (grant 2016 FI_B1 00019), and Centro de Láseres Pulsados (CLPU) for granting access to its facilities.

Author details

María-Victoria Collados[1], Íñigo J. Sola[2], Julia Marín-Sáez[1,3], Warein Holgado[2,4] and Jesús Atencia[1]*

*Address all correspondence to: atencia@unizar.es

1 Applied Physics Department, Aragon Institute of Engineering Research (I3A), University of Zaragoza, Zaragoza, Spain

2 Photonics and Laser Applications Group, Applied Physics Department, University of Salamanca, Salamanca, Spain

3 Enviromental Sciences Departament, Applied Physics Section, University of Lleida, Lleida, Spain

4 Pulsed Lasers Center (CLPU), Villamayor (Salamanca), Spain

References

[1] J. E. Curtis, B. A. Koos, and D. G. Grier. Dynamic holographic optical tweezers. Optics Communications. 2002;**207**(1–6):169–175. DOI: 10.1016/S0030-4018(02)01524-9

[2] G. A. Swartzlander Jr. The Optical Vortex Lens. Optics & Photonics News. 2006;**17**(11):34–41. DOI: 10.1364/OPN.17.11.000039

[3] M. S. Bigelow, P. Zerom, and R. W. Boyd. Breakup of ring beams carrying orbital angular momentum in sodium vapor. Physical Review Letters. 2004;**92**(8):083902. DOI: 10.1103/PhysRevLett.92.083902

[4] Z. Chen, M. Shih, M. Segev, D. W. Wilson, R. E. Muller, and P. D. Maker. Steady-state vortex-screening solitons formed in biased photorefractive media. Optics Letters. 1997;**22**(23):1751–1753. DOI: 10.1364/OL.22.001751

[5] M. Fisher, C. Siders, E. Johnson, O. Andrusyak, C. Brown, and M. Richardson. Control of filamentation for enhancing remote detection with laser induced breakdown spectroscopy. Proceedings of SPIE. 2006;**6219**:621907. DOI: 10.1117/12.663824

[6] J. Courtial, M. J. Padgett. Performance of a cylindrical lens mode converter for producing Laguerre-Gaussian laser modes. Optics Communications. 1999;**159**(1–3):13–18. DOI: 10.1016/S0030-4018(98)00599-9

[7] J. A. Rodrigo, T. Alieva, and M. L. Calvo. Experimental implementation of the gyrator transform. Journal of the Optical Society of America A. 2007;**24**(10):3135–3139. DOI: 10.1364/JOSAA.24.003135

[8] K. Sueda, G. Miyaji, N. Miyanaga, and M. Nakatsuka. Laguerre-Gaussian beam generated with a multilevel spiral phase plate for high intensity laser pulses. Optics Express. 2004;**12**(15):3548–3553. DOI: 10.1364/OPEX.12.003548

[9] W. C. Cheong, W. M. Lee, X-C Yuan, L-S Zhang, K. Oholakia, and H. Wang. Direct electron-beam writing of continuous spiral phase plates in negative resist with high power efficiency for optical manipulation. Applied Physics Letters. 2004;**85**:5784–5786. DOI: 10.1063/1.1830678

[10] J. W. Sung, H. Hockel, J. D. Brown, and E. G. Johnson. Development of a two-dimensional phase-grating mask for fabrication of an analog-resist profile. Applied Optics. 2006;**45**(1):33–43. DOI: 10.1364/AO.45.000033

[11] K. J. Moh, X-C Yuan, D. Y. Tang, W. C. Cheong, L-S Zhang, D. K. Y. Low, X. Peng, H. B. Niu, and Z. Y. Lin. Generation of femtosecond optical vortices using a single refractive optical element. Applied Physics Letters. 2006;**88**:091103. DOI: 10.1063/1.2178507

[12] G. A. Swartzlander Jr. Achromatic optical vortex lens. Optics Letters. 2006;**31**(13):2042–2044. DOI: 10.1364/OL.31.002042

[13] V. Y. Bazhenov, M. S. Soskin, and M. V. Vasnetsov. Screw dislocations in light wavefronts. Journal of Modern Optics. 1992;**39**(5):985–990. DOI: 10.1080/09500349214551011

[14] H. He, N. R. Heckenberg, and H. Rubinsztein-Dunlop. Optical particle trapping with higher-order doughnut beams produced using high efficiency computer generated holograms. Journal of Modern Optics. 1995;**42**(1):217–223. DOI: 10.1080/09500349514550171

[15] K. Crabtree, J. A. Davis, and I. Moreno. Optical processing with vortex-producing lenses. Applied Optics. 2004;**43**(6):1360–1367. DOI: 10.1364/AO.43.001360

[16] Z. S. Sacks, D. Rozas, and G. A. Swartzlander. Holographic formation of optical-vortex filaments. Journal of the Optical Society of America B. 1998;**15**(8):2226–2234. DOI: 10.1364/JOSAB.15.002226

[17] I. G. Mariyenko, J. Strohaber, and C. J. G. J. Uiterwaal. Creation of optical vortices in femtosecond pulses. Optics Express. 2005;**13**(19):7599–7608. DOI: 10.1364/OPEX.13.007599

[18] K. Bezuhanov, A. Dreischuh, G. G. Paulus, M. G. Schätzel, and H. Walther. Vortices in femtosecond laser fields. Optics Letters. 2004;**29**(16):1942–1944. DOI: 10.1364/OL.29.001942

[19] I.J. Sola, V. Collados, L. Plaja, C. Méndez, J. San Román, C. Ruiz, I. Arias, A. Villamarín, J. Atencia, M. Quintanilla, and L. Roso. High power vortex generation with volume phase holograms and non-linear experiments in gases. Applied Physics B. 2008;**91**(1):115–118. DOI: 10.1007/s00340-008-2967-9

[20] A. Villamarín, J. Atencia, M.V. Collados, and M. Quintanilla. Characterization of transmisión volume holographic gratings recorded in Slavich PFG04 dichromated gelatin plates. Applied Optics. 2009;**48**(22):4348–4353. DOI: 10.1364/AO.48.004348

[21] O. Martínez–Matos, J. A. Rodrigo, M. P. Hernández-Garay, J. G. Izquierdo, R. Weigand, M. L. Calvo, P. Cheben, P. Vaveliuk, and L. Bañares. Generation of femtosecond paraxial beams with arbitrary spatial distribution. Optics Letters. 2010;**35**(5):652–654. DOI: 10.1364/OL.35.000652

[22] J. Atencia, M. V. Collados, M. Quintanilla, J. Marín-Sáez, and I. J. Sola. Holographic optical element to generate achromatic vortices. Optics Express. 2013;**21**(18):21056–21061. DOI: 10.1364/OE.21.021056

[23] H. Kogelnik. Coupled wave theory for thick hologram gratings. Bell System Technical Journal. 1969;**48**(9):2909–2947. DOI: 10.1002/j.1538-7305.1969.tb01198.x

[24] R. J. Collier, C. H. Burckhardt, and L. H. Lin. Optical Holography. 1st ed. New York: Academic Press; 1971. 605 p.

[25] A. Villamarín, I. J. Sola, M. V. Collados, J. Atencia, O. Varela, B. Alonso, C. Méndez, J. San Román, I. Arias, L. Roso, and M. Quintanilla. Compensation of second-order dispersion in femtosecond pulses after filamentation using volume holographic transmission gratings recorded in dichromated gelatin. Applied Physics B. 2012;**106**(1):135–141. DOI: 10.1007/s00340-011-4770-2

[26] J. W. Goodman. Introduction to Fourier Optics. 2nd ed. Singapore: McGraw-Hill; 1996. 441 p.

[27] M. Miranda, M. Kotur, P. Rudawski, C. Guo, A. Harth, A. L'Huillier and C. L. Arnold. Spatiotemporal characterization of ultrashort optical vortex pulses. Journal of Modern Optics. 2016. DOI: 10.1080/09500340.2016.1257751

[28] K. T. Kim, C. Zhang, A. D. Shiner, B. E. Schmidt, F. Légaré, D. M. Villeneuve, and P. B. Corkum. Petahertz optical oscilloscope. Nature Photonics. 2007;**13**:958–962. DOI: 10.1038/nphoton.2013.286

[29] C. Ruiz, J. San Román, C. Méndez, V. Díaz, L. Plaja, I. Arias, and L. Roso. Observation of Spontaneous Self-Channeling of Light in Air below the Collapse Threshold. Physical Review Letters. 2005;**95**:053905. DOI: 10.1103/PhysRevLett.95.053905

[30] A. Couairon and A. Mysyrowicz. Femtosecond filamentation in transparent media. Physics Reports. 2007;**441**(2–4):47–189. DOI: 10.1016/j.physrep.2006.12.005

[31] P. B. Corkum and F. Krausz. Attosecond science. Nature Physics. 2007;**3**:381–387. DOI: 10.1038/nphys620

[32] T. Popmintchev, M.-C. Chen, D. Popmintchev, P. Arpin, S. Brown, S. Alisauskas, G. Andriukaitis, T. Balciunas, O. D. Muecke, A. Pugzlys, A. Baltuska, B. Shim, S. E. Schrauth, A. Gaeta, C. Hernandez-Garcia, L. Plaja, A. Becker, A. Jaron-Becker, M. M. Murnane, and H. C. Kapteyn. Bright coherent ultrahigh harmonics in the keV X-ray regime from mid-infrared femtosecond lasers. Science. 2012;**336**(6086):1287–1291. DOI: 10.1126/science.1218497

[33] P. B. Corkum. Plasma perspective on strong field multiphoton ionization. Physical Review Letters. 1993;**71**(13):1994-1997. DOI: 10.1103/PhysRevLett.71.1994

[34] K. Schafer, B. Yang, L.F. DiMauro, and K.C. Kulander. Above threshold ionization beyond the high harmonic cutoff. Physical Review Letters. 1993;**70**:1599. DOI: 10.1103/PhysRevLett.70.1599

[35] M. Hentschel, R. Kienberger, C. Spielmann, G. A. Reider, N. Milosevic, T. Brabec, P. Corkum, U. Heinzmann, M. Drescher, and F. Krausz. Attosecond metrology. Nature. 2001;**414**:509–513. DOI: 10.1038/35107000

[36] G. Sansone, E. Benedetti, F. Calegari, C. Vozzi, L. Avaldi, R. Flammini, L. Poletto, P. Villoresi, C. Altucci, R. Velotta, S. Stagira, S. De Silvestri, and M. Nisoli. Isolated single-cycle attosecond pulses. Science. 2006;**314**(5798):443–446. DOI: 10.1126/science.1132838

[37] I. J. Sola, E. Mevel, L. Elouga, E. Constant, V. Strelkov, L. Poletto, P. Villoresi, E. Benedetti, J. P. Caumes, S. Stagira, C. Vozzi, G. Sansone, and M. Nisoli. Controlling attosecond electron dynamics by phase-stabilized polarization gating. Nature Physics. 2006;**2**:319–322. DOI: 10.1038/nphys281

[38] M. Zürch, C. Kern, P. Hansinger, A. Dreischuh, and C. Spielmann. Strong-field physics with singular light beams. Nature Physics. 2012;**8**:743–746. DOI: 10.1038/nphys2397

[39] C. Hernandez-Garcia, A. Picon, J. San Roman, and L. Plaja. Attosecond extreme ultraviolet vortices from high-order harmonic generation. Physics Review Letters. 2013;**111**:083602. DOI: 10.1103/PhysRevLett.111.083602

[40] G. Gariepy, J. Leach, K. T. Kim, T.J. Hammond, E. Frumker, R. W. Boyd, and P.B. Corkum. Creating high-harmonic beams with controlled orbital angular momentum. Physics Review Letters. 2014;**113**:153901. DOI: 10.1103/PhysRevLett.113.153901

[41] L. Rego, J. San-Román, L. Plaja, A. Picón, and C. Hernández-García. Ultrashort extreme-ultraviolet vortices. In: H. Pérez-de-Tejada, editor. Vortex Dynamics. 1st ed. Rijeka: Intech; 2016.

IntechOpen

IntechOpen

IntechOpen